Myocardial Deformation from Local Frequency Estimation in Tagging MRI

L.C.M. Bruurmijn[1], H.B. Kause[2], O.G. Filatova[2], R. Duits[1,3], A. Fuster[1,3], L.M.J. Florack[1,3], and H.C. van Assen[2]

[1] Department of Biomedical Engineering
[2] Department of Electrical Engineering
[3] Department of Mathematics & Computer Science
Eindhoven University of Technology, The Netherlands (www.iste.nl)

Abstract. We consider a new method to analyse deformation of the myocardial wall from tagging magnetic resonance images. The method exploits the fact that a regular pattern of stripe tags induces a time-dependent frequency covector field tightly coupled to the myocardial tissue and not affected by tag fading. The corresponding local frequency can be disambiguated with the help of the Gabor transform. The transformation of the tagging frequency covector field is governed by the deformation tensor field. Reversely, the deformation (and strain) tensor field can be retrieved from local frequency estimates given at least n (independent) tagging sequences, where n denotes spatial dimension. For the sake of illustration we consider the conventional case $n = 2$. Moreover, we make use of an overdetermined system by exploiting 4 instead of 2 tagging directions, which contributes to the robustness of the results. The method does not require explicit knowledge of material motion or tag line extraction. Displacement estimations are compared to HARP.

Keywords: Tagging Magnetic Resonance Imaging, Myocardial Deformation, Gabor Transform, Cardiac Image Analysis

1 Introduction

Tagging Magnetic Resonance Imaging (tMRI) [1, 2] can reveal important quantitative information on (early) stages of cardiac dysfunction that are difficult to observe using other imaging techniques [3, 4]. Myocardial function may be affected by cardiac infarction, hypertension, or underperfusion of the cardiac muscle. An accurate motion or deformation field provides a basis for the assessment of myocardial function.

Heart wall *deformation* can be obtained from the *motion gradient* [5], or by tracking tag lines [6]. Motion extraction algorithms must be able to cope with tag fading caused by spin-lattice relaxation. This fact has led to other approaches,

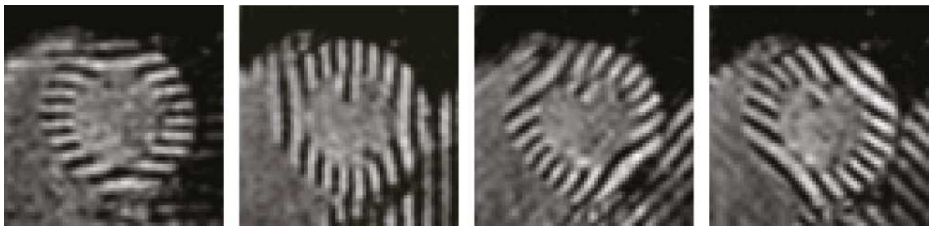

Fig. 1. Short-axis tMRI images of a left ventricle in systole using four tag directions. Images courtesy of dr. Jos Westenberg, LUMC, Leiden, The Netherlands.

such as modeling the tag fading explicitly [7], or exploiting phase constancy [8, 9]. HARP (Harmonic Phase) [10] is a tracking technique which extracts the phase of a SPAMM-tagged image [2] by bandpass-filtering around the first harmonic spectral peak near the typical tagging frequency using Gabor filters.

We introduce a new method to estimate heart wall deformation. We pursue an approach similar to those proposed in [4, 11], based on *local frequency* estimation. Instead of Gabor or log-normal quadrature filters, we employ a generalized wavelet transform, viz. the Gabor transform, to construct a local tag frequency representation from which subsequently the required local frequency covector fields are extracted. Whereas in [11] strains are calculated from displacements, we do not require the latter. Since this method exploits frequency instead of amplitude information, it is robust to tag fading. Moreover, the method is designed to work with any number A of tag directions ($A \geq n$). If $A > n$ an overdetermined system of equations results. In this study myocardial deformation is assessed using stripe tags in $A = 2$ and 4 directions (Fig. 1). The deformation tensor is used to calculate radial, circumferential and shear components of the Lagrangian strain tensor, which are clinically accepted measures for deformation.

The paper is organized as follows. Section 2 treats local frequency analysis by the Gabor transform. Section 3 introduces the proposed method to calculate myocardial deformation. In Section 4 we present results on artificial tMRI data. Finally, we conclude with a discussion in Section 5.

2 Local Frequency Analysis

To capture *local* frequency characteristics, Gabor proposed an expansion into translated and modulated, spatially confined basis functions (the Gabor window) [12]. In the continuous case, this Gabor transform reads

$$G(\mathbf{p}, \boldsymbol{\omega}) = \int_{\mathbb{R}^2} f(\mathbf{q}) \overline{\psi(\mathbf{q} - \mathbf{p})} \mathrm{e}^{-2\pi \mathrm{i}(\mathbf{q}-\mathbf{p})\cdot\boldsymbol{\omega}} \mathrm{d}\mathbf{q} \tag{1}$$

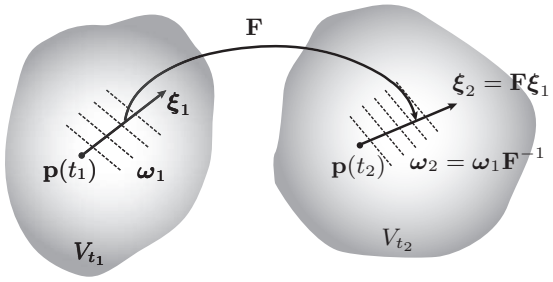

Fig. 2. The deformation gradient tensor $\mathbf{F}$ maps an infinitesimal vector $\boldsymbol{\xi}_1$ (represented by the arrow) in configuration V_{t_1} into $\boldsymbol{\xi}_2$ in configuration V_{t_2}. The transformation of the frequency covectors $\boldsymbol{\omega}_1$ and $\boldsymbol{\omega}_2$ (dashed lines) is also induced by $\mathbf{F}$ (namely, $\mathbf{F}^{-1}$).

where $f : \mathbb{R}^2 \to \mathbb{R}$ is the 2-dimensional tagging image, $\psi : \mathbb{R}^2 \to \mathbb{C}$ the Gabor window, $\overline{\psi}$ denotes its complex conjugate and $\mathbf{p}, \boldsymbol{\omega} \in \mathbb{R}^2$ are position and spatial frequency respectively. We apply this transform for every time frame and every tag direction. A Gaussian window is chosen for ψ, for this has the best position–frequency localisation [12]. The Gabor transform can be efficiently implemented using the Zak transform [13].

The Gabor transform offers a position–frequency representation of an image. For our application we extract a single frequency covector $\boldsymbol{\omega}(\mathbf{p}(t), t)$ at each position $\mathbf{p}(t) = (\mathbf{x}(t), \mathbf{y}(t))$ and time frame t, and for each tag direction (for ease of notation we shall write $\boldsymbol{\omega}$):

$$\boldsymbol{\omega} = \omega_x \, \mathrm{d}\mathbf{x} + \omega_y \, \mathrm{d}\mathbf{y} \tag{2}$$

3 Calculating Deformation from Local Frequency

Let us denote the tissue configuration at two distinct moments of time t_1 and $t_2 > t_1$ by V_{t_1} and V_{t_2} respectively. Consider a point in the reference configuration, $\mathbf{p}(t_1) \in V_{t_1}$, and its infinitesimal neighbourhood, and a vector $\boldsymbol{\xi}_1$ connecting $\mathbf{p}(t_1)$ to some point in this neighbourhood. In the deformed configuration $(\mathbf{p}(t_1), \boldsymbol{\xi}_1)$ is mapped to $(\mathbf{p}(t_2), \boldsymbol{\xi}_2)$ with $\mathbf{p}(t_2) \in V_{t_2}$. The *deformation tensor* [14] is the linear mapping $\mathbf{F} = \mathbf{F}|_{(\mathbf{p}(t_1), t_1)}$, such that

$$\boldsymbol{\xi}_2 = \mathbf{F}\boldsymbol{\xi}_1 \tag{3}$$

In an infinitesimally small neighbourhood the global tag pattern at time t_1 can be considered as a constant frequency pattern. At time t_2 this frequency pattern is deformed relative to the reference tissue configuration. For a geometrical intuition see Fig. 2, where we depict vectors $\boldsymbol{\xi}$ as arrows and frequency covectors

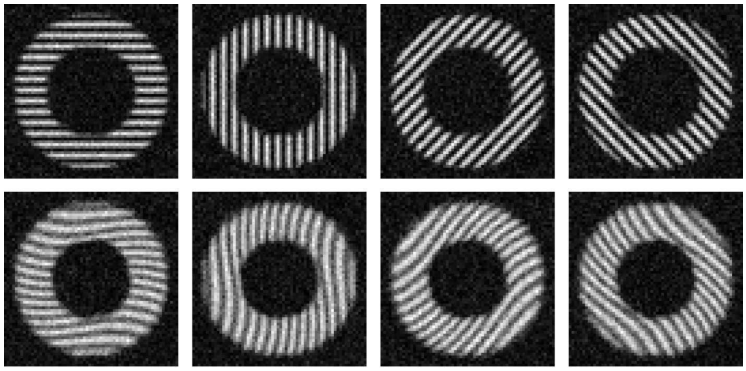

Fig. 3. Artificial tMRI data of a short-axis view of the left ventricle for all tag directions at begin and end systole.

$\boldsymbol{\omega}$ as (dashed) equidistant lines with normals in the direction of the frequency and spacing inversely proportional to the frequency magnitude. (The frequency covector lines coincide with the local tag pattern.) Using this representation, $\langle \boldsymbol{\omega}, \boldsymbol{\xi} \rangle \in \mathbb{R}$ can be defined as the number of $\boldsymbol{\omega}$-lines pierced by the vector $\boldsymbol{\xi}$. The number of pierced lines remains constant, i.e. $\langle \boldsymbol{\omega}_1, \boldsymbol{\xi}_1 \rangle = \langle \boldsymbol{\omega}_2, \boldsymbol{\xi}_2 \rangle$, inducing the covector transformation law by virtue of Eq. (3)

$$\boldsymbol{\omega}_2 = \boldsymbol{\omega}_1 \mathbf{F}^{-1} \tag{4}$$

where $\boldsymbol{\omega}_1$ and $\boldsymbol{\omega}_2$ represent the local frequencies in $(\mathbf{p}(t_1), t_1)$ and $(\mathbf{p}(t_2), t_2)$.

Recall that $\boldsymbol{\omega}_1$ and $\boldsymbol{\omega}_2$ need to be evaluated at *corresponding* material points, $(\mathbf{p}(t_1), t_1)$ and $(\mathbf{p}(t_2), t_2)$. However, the relation between $\mathbf{p}(t_1)$ and $\mathbf{p}(t_2)$ is not known, since we do not compute material motion. One way to overcome this is to assume a slowly varying frequency field and apply linear deformation theory between successive time frames, so that $\mathbf{p}(t_2) \approx \mathbf{p}(t_1)$. Although this allows to approximate $\mathbf{F}$ from Eq. (5), induced errors will accumulate. In order to avoid this, we assume that at the fiducial moment t_0 when the tag pattern is applied in the scanner frequency is a known, global constant. We use this (unobserved) configuration at time t_0 as reference.

Because a tMRI acquisition typically consists of at least two encoding directions, Eq. (4) constitutes a system of equations that can be compactly written as

$$\boldsymbol{\Omega}_{t_2} = \boldsymbol{\Omega}_{t_1} \mathbf{F}^{-1}, \text{ with } \boldsymbol{\Omega} = \begin{bmatrix} \boldsymbol{\omega}^1 \\ \vdots \\ \boldsymbol{\omega}^A \end{bmatrix} \tag{5}$$

with upper indices $1, \ldots, A$ enumerating tag directions. The deformation tensor at point $\mathbf{p}(t)$ at time t relative to t_0 can then be calculated as

$$\mathbf{F} = \left(\boldsymbol{\Omega}_t^T \boldsymbol{\Omega}_t \right)^{-1} \boldsymbol{\Omega}_t^T \boldsymbol{\Omega}_{t_0} \tag{6}$$

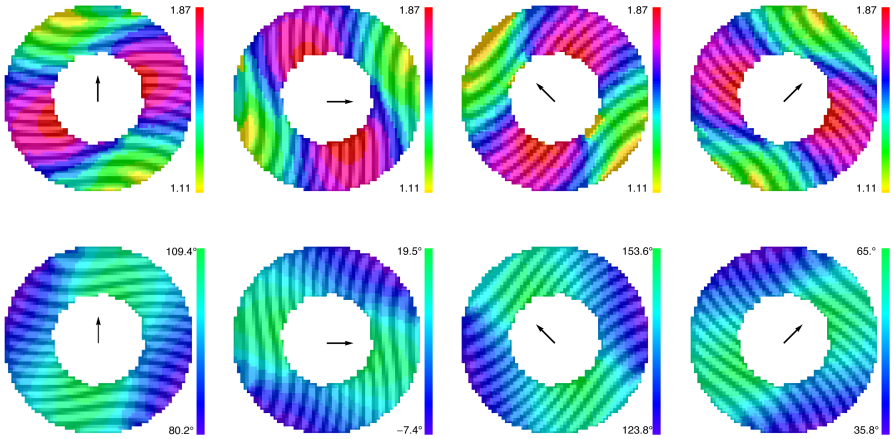

Fig. 4. Top: Tag images overlaid with a pixelwise representation of the magnitudes of the estimated local frequency vectors (colours) obtained from the Gabor transform for four tag directions in mid-systole. Bottom: Tag images overlaid with the corresponding local frequency vector directions. Arrows show the initial tag frequency direction.

where T denotes transposed. The Lagrangian strain tensor is

$$\mathbf{E} = \frac{1}{2}(\mathbf{F}^T\mathbf{F} - \mathbf{I}) \tag{7}$$

One can extract circumferential (E_{cc}), radial (E_{rr}) and shear (E_{cr}) strains

$$E_{cc} = \hat{\mathbf{e}}_c^T\,\mathbf{E}\,\hat{\mathbf{e}}_c\ ,\ E_{rr} = \hat{\mathbf{e}}_r^T\,\mathbf{E}\,\hat{\mathbf{e}}_r\ ,\ E_{cr} = \hat{\mathbf{e}}_c^T\,\mathbf{E}\,\hat{\mathbf{e}}_r \tag{8}$$

with local unit radial and circumferential basis vectors $\hat{\mathbf{e}}_r$ and $\hat{\mathbf{e}}_c$.

The numerical implementation consists of the following steps:

i Calculate the Gabor transform $G(\mathbf{p}(t), \boldsymbol{\omega}(t))$, Eq. (1), for all tag directions, using a Gaussian filter ψ with $\sigma = 4$.
ii Determine the local frequency $\boldsymbol{\omega}$ with highest intensity in the Gabor domain, excluding the zero-frequency peak.
iii Compute the deformation tensor $\mathbf{F}$, Eq. (6) for every time t, relative to the reference time t_0.
iv Calculate the strain tensor $\mathbf{E}$, Eq. (7), and components E_{rr}, E_{cc} and E_{cr}, Eq. (8).

4 Experimental Results

Artificial tMRI data consist of a series of 16 frames (64×64 pixels) of contracting and rotating rings, simulating the systolic phase in a single short-axis slice of

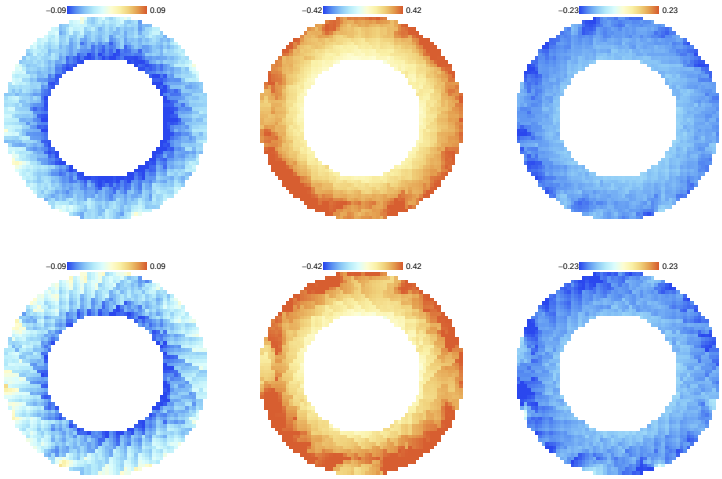

Fig. 5. Short-axis view of circumferential (left), radial (middle), and shear (right) components of the Lagrangian strain tensor in the left ventricle computed in mid-systole. Top row: Using four tag directions. Bottom row: Using two tag directions.

the left-ventricle, with two and four tagging directions ($A=2,4$), see Fig. 3. The wall thickens and rotation varies radially, causing the endocardium to rotate more than the epicardium, inducing shear deformation. Tag fading is modeled by exponential decay and Rician noise is added.

For one volunteer, a short-axis slice of the left-ventricle was acquired in 30 frames with SPAMM imaging, forming a whole heart cycle. Data was acquired for four tag directions ($A=4$) with a tag size of 7 mm. Image acquisition was performed with a 3T MRI scanner (Achieva, Philips Medical Systems) after informed con-

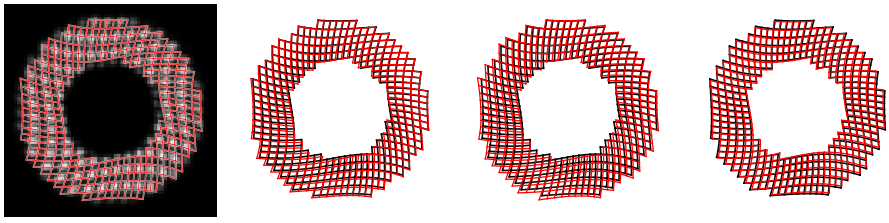

(a) (b) (c) (d)

Fig. 6. (a) Image with horizontal and vertical tags combined for visualisation, overlaid with deformed lattice calculated from four tag directions in a mid-systolic frame. (b,c,d) Comparison of the true deformed grid (black) and deformed grid (red) calculated using four tag directions (b), two tag directions (c), and HARP using two tag directions (d). HARP based on four tag directions gave quite similar results.

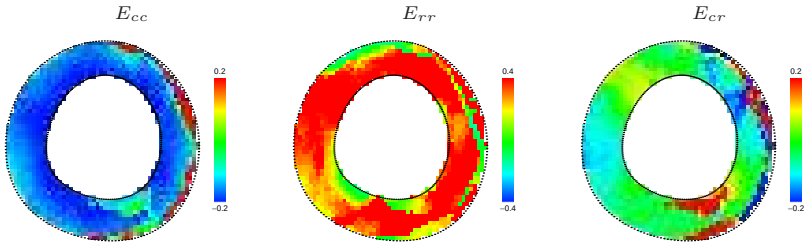

Fig. 7. Strain at end systole computed from a volunteer MRI data set (A=4).

sent and with permission from the Medical Ethical Committee. A 2D multi-shot gradient-echo with Echo Planar Imaging with breath holding in end-expiration was used. Scan parameters: TE 3.2 ms, TR 6.3 ms, flip angle 10°, acquisition voxel size $1.34 \times 1.34 \times 10$ mm^3.

Local frequencies (Eq. (2)) are calculated for all time steps and tag directions (see Fig. 4), deformation tensors are calculated according to Eq. (6). These are used to calculate radial, circumferential and shear strains, using four and two tag directions respectively (see Fig. 5). For a large number of points organised in a rectangular grid (see Fig. 6), their displacements were calculated based on the deformation tensors from Eq. (6) and by our own implementation of HARP [10], using both four and two tag directions. We adapted HARP to accept four input image sequences. Average displacement errors for the grid points in the mid-systolic frame using our novel method were 0.47 ± 0.23 and 0.68 ± 0.26 pixels for four and two tag directions respectively. For HARP using both four and two tag directions, these errors were 0.54 ± 0.07 and 0.53 ± 0.07 pixels respectively.

Fig. 7 shows the volunteer strain plots at end systole based on four tag directions.

5 Discussion and Conclusion

Quantitative myocardial deformation has been obtained accurately and robustly from a Gabor frequency analysis of artificial tMRI data using four tag directions. In contemporary medical practice it is common to use two tag directions. The use of more directions for the analysis leads to more stable and more homogeneous results (Fig. 5). A visualisation of the strain components shows the expected behaviour. Additionally, Fig. 4 shows that the Gabor analysis results in a smooth frequency profile. The method does neither require explicit knowledge of material motion nor tag line extraction. Moreover, it is robust to tag fading and can be straightforwardly generalised to any number of tagging directions and to volumetric tagging data. Subsequent approximation of tissue displacements performs comparably to HARP, while using four tag directions gives better results than using two. Since HARP is an iterative approach minimising phase differences, using four tag directions does not improve HARP's results. Like HARP,

adding an iterative component may improve our method. Another improvement may possibly be obtained by optimisation of the tagging configuration during image acquisition for frequency extraction using the Gabor transform.

References

1. Zerhouni, E.A., Parish, D.M., Rogers, W.J., Yang, A., Shapiro, E.P.: Human heart: Tagging with MR imaging—a method for noninvasive assessment of myocardial motion. Radiology **169**(1) (1988) 59–63
2. Axel, L., Dougherty, L.: MR imaging of motion with spatial modulation of magnetization. Radiology **171**(3) (1989) 841–845
3. Götte, M.J., van Rossum, A.C., Twisk, J.W.R., Kuijer, J.P.A., Marcus, J.M., Visser, C.A.: Quantification of regional contractile function after infarction: Strain analysis superior to wall thickening analysis in discriminating infarct from remote myocardium. Journal of the American College of Cardiology **37** (2001) 808–817
4. Qian, Z., Liu, Q., Metaxas, D., Axel, L.: Identifying regional cardiac abnormalities from myocardial strains using non-tracking-based strain estimation and spatio-temporal tensor analysis. IEEE Transactions on Medical Imaging **30**(12) (2011) 2017 – 2029
5. Florack, L., van Assen, H.: A new methodology for multiscale myocardial deformation and strain analysis based on tagging MRI. International Journal of Biomedical Imaging (2010) Published online: DOI 10.1155/2010/341242.
6. Smal, I., Carranza-Herrezuelo, N., Klein, S., Niessen, W., Meijering, E.: Quantitative comparison of tracking methods for motion analysis in tagged MRI. In: Proceedings of the 8th IEEE International Symposium on Biomedical Imaging: From Nano to Macro, ISBI 2011, March 30 - April 2, 2011, Chicago, Illinois, USA. (April 2011) 345–348
7. Gupta, S.N., Prince, J.L.: On variable brightness optical flow for tagged MRI. In Bizais, Y., ed.: Proceedings of the Fourteenth International Conference on Information Processing in Medical Imaging–IPMI 1995 (Ile de Berder, France), Dordrecht, Kluwer Academic Publishers (1995) 323–334
8. Van Assen, H., Florack, L., Simonis, F., Westenberg, J., Strijkers, G.: Cardiac strain and rotation analysis using multi-scale optical flow. In Wittek, A., Nielsen, P.M.F., Miller, K., eds.: Computational Biomechanics for Medicine V, Springer-Verlag (2010) 89–100
9. Garcia-Barnés, J., Gil, D., Pujadas, S., Carreras, F.: Variational framework for assessment of the left ventricle motion. Mathematical Modelling of Natural Phenomena **3**(6) (2008) 76–100
10. Osman, N.F., McVeigh, E.R., Prince, J.L.: Imaging heart motion using harmonic phase MRI. IEEE Transactions on Medical Imaging **19**(3) (2000) 186–202
11. Arts, T., Prinzen, F.W., Delhaas, T., Milles, J.R., Rossi, A.C., Clarysse, P.: Mapping displacement and deformation of the heart with local sine-wave modeling. IEEE Transactions on Medical Imaging **29**(5) (May 2010)
12. Duits, R., Führ, H., Janssen, B., Bruurmijn, M., Florack, L., van Assen, H.: Evolution equations on Gabor transforms and their applications. Applied and Computational Harmonic Analysis (2012) http://dx.doi.org/10.1016/j.acha.2012.11.007.
13. Janssen, A.: The Zak transform: A signal transform for samples time-continuous signals. Philips Journal of Research **43**(1) (1988) 23–69
14. Haupt, P.: Continuum Mechanics and Theory of Materials. Springer-Verlag, Berlin (2002)